Journal of Materials Chemistry C

PAPER

Check for updates

A Cu₂I₂ cluster bearing MOF as a fluorescence-sensing material for the visual detection of methanol

Nian-Hao Wang,[ab] Jin-Mei Liu,[ab] Abdusalam Ablez,[ab] Lin-Xu Tian,[ab] Yi Liu,[ab] Bin Tan,[c] Zhao-Feng Wu [ID] *[a] and Xiao-Ying Huang [ID] [a]

Due to their wide applications with regard to health and safety, sensitive and selective detection and distinguishing of alcohol molecules (*e.g.*, methanol in counterfeit wine) is very important. Fluorescence (FL)-sensing materials towards probing alcohol molecules have been extensively developed based on their advantages of economy, convenience, and rapid detection. Herein, a fluorescent metal–organic framework (FL MOF) Cu₂I₂(pdc)₄Sr₄(DMF)₆ (Sr-CuI-MOF, H₂pdc = 3,5-pyridinedicarboxylic acid) featuring a three-dimensional (3D) structure was characterized. Sr-CuI-MOF exhibited a thermally activated delayed fluorescence arising from the Cu₂I₂-pdc motif. Upon exposure to methanol, Sr-CuI-MOF showed a sensitive and selective fluorescence redshift, characterized by a pronounced solvatochromism. Consequently, Sr-CuI-MOF could be used to accurately detect methanol by analyzing the linear relationship between the shift in emission wavelength or percentage of the fluorescence intensity quenching and methanol concentration. It represents the first CuI-bearing MOF with fluorescence detection of methanol. This work presents a novel approach to design FL-sensing MOFs that can be seen by the naked eye utilizing CuI-ligand motifs as building blocks and emission centers.

1. Introduction

The breakdown of methanol can produce harmful compounds such as formaldehyde and formic acid. Prolonged exposure to methanol can result in permanent harm to the human nervous system and, in extreme cases, may be fatal. Moreover, due to its resemblance to ethanol and its cost-effectiveness, methanol is often mixed into ethanol fuels and fake alcoholic drinks, which presents serious risks to public health and safety.[1–4] Therefore, detection of methanol is of great importance. Traditional methods for detecting methanol mainly depend on chemiresistive sensors,[5,6] nuclear magnetic resonance (NMR)[7,8] spectroscopy and liquid chromatography (LC).[9] Nonetheless, the relatively high expense, operational difficulties, extended analysis time, and other factors would restrict their use, particularly in remote areas. Fluorescence (FL) sensing has emerged as a promising method due to its advantages of convenience, efficiency, and cost-effectiveness. By creating a linear relationship between the luminescence intensity or position of FL materials and the concentration of analytes, a sensitive FL array can be developed.[10–13] Consequently, creating

sensitive and selective FL-sensing materials that are sensitive and selective is an important, yet challenging, task.

Metal–organic frameworks (MOFs) have recently shown significant promise in FL-sensing applications because of their adjustable porosity, diverse luminescent characteristics, and their ability to selectively and sensitively detect towards specific analytes.[11,14–17] However, due to their chemical similarities, there are few reports on MOFs that exhibit selective FL sensing for methanol compared with other interfering alcohols.[18–21] In particular situations such as antifreeze, non-contact fuels, and industrial synthetic processes, a specific amount of methanol is allowed. Nevertheless, MOF-based sensing materials are solely designed for the specific detection of trace amounts of methanol, as even small quantities can affect the luminescent characteristics of the material. This makes it impossible for them to adequately recognize methanol in proportion.[18–21] As a result, creating new fluorescent MOFs that can specifically identify methanol is highly important scientifically and practically. There have been no reports on the selective detection of methanol in mixtures with other alcohols and specifically ethanol.

In this work, a novel three-dimensional (3D) MOF of {Cu₂I₂-(pdc)₄Sr₄(DMF)₆}ₙ (denoted as Sr-CuI-MOF, where H₂pdc = 3,5-pyridinedicarboxylic acid) assembled from strontium (Sr), CuI, and H₂pdc ligands was synthesized and characterized. By using Cu₂I₂(pdc)₄ units as luminescent centers, Sr-CuI-MOF exhibited significant fluorescence quenching towards in the presence of methanol, which was accompanied by a noticeable shift in

a Fujian Institute of Research on the Structure of Matter, The Chinese Academy of Sciences, Fuzhou, Fujian, 350002, China. E-mail: zfwu@fjirsm.ac.cn
b Fujian College, University of Chinese Academy of Sciences, Fuzhou 350002, P. R. China
c School of Chemistry and Chemical Engineering, Beijing Institute of Technology, Beijing 102488, P. R. China

This journal is © The Royal Society of Chemistry 2025

J. Mater. Chem. C, 2025, **13**, 22263–22270 | **22263**

emission colour from green to orange. This phenomenon allowed for clear differentiation of methanol (in gas and liquid forms) from ethanol and other typical alcohols. The simultaneous FL quenching and emission redshift through a dual-response mechanism confirmed that Sr-CuI-MOF could be used for the specific recognition of methanol. The results obtained from liquid chromatography-mass spectrometry (LC-MS), elemental analyses, and powder X-ray diffraction indicated that the sensing mechanism originated from the partial exchange of terminal DMF molecules with methanol. Few MOFs for detecting methanol have been documented,[20,22–24] while the ability to visually identify methanol continues to be a difficult (but important) challenge. We believe this work will offer a new approach for creating FL-sensing MOFs with emissive CuI modules to assess the quality of commercial wine and ethanol fuel.

2. Experimental

2.1. Materials and methods

All reagents and chemicals were purchased from commercial sources and used without further purification. Powder X-ray diffraction (PXRD) patterns were recorded on a Rigaku MiniFlex II diffractometer using Cu Kα radiation ($\lambda = 1.54178$ Å). A graphite monochromator was used and the generator power settings were set at 44 kV and 40 mA. Data were collected between 2θ of 5–50° with a scanning speed of 0.5° min^{-1}. Single-crystal X-ray diffraction data (SCXRD) were collected with a Rigaku XtaLAB Synergy CCD diffractometer using graphite-monochromated Cu Kα radiation ($\lambda = 1.54178$ Å) at 298 K. Multi-temperature FL spectroscopy was undertaken on an FLS1000 spectrometer. Energy-dispersive spectroscopy (EDS) with mapping was done on a Zeiss Sigma 300 scanning electron microscope with an accelerating voltage of 3 kV. The instrument used for X-ray photoelectron spectroscopy (XPS) was a Thermo Scientific ESCALAB 250 Xi with a monochromatic A1 Kα X-ray source (1486.6 eV) operating at 15 kV; the substrate pressure was 5.0×10^{-8} Pa. All peaks were corrected with the characteristic peaks of C 1s (binding energy = 284.8 eV), and the peak fits were analysed by Avantage 5.932 software. UV-vis diffuse reflectance data were collected on a Shimadzu UV-2600 UV-visible spectrophotometer with the wavelength range set from 200 nm to 800 nm. The multi-temperature FL spectra of Gd-CuI-MOF at the solid state were obtained on an FLS1000 spectrometer. Sensing performances were recorded using an FLS980 spectrometer, while the cycling experiments and sensing capacities to alcoholic wines and fuel simulants were conducted on a PerkinElmer LS55 fluorescence spectrometer.

2.2. X-ray crystallography

A single crystal of compound Sr-CuI-MOF suitable for SCXRD was selected under an optical microscope and glued to a thin glass fiber. The structure was solved by direct methods and refined with full-matrix least-squares techniques using the SHELX2018 package.[25] The CCDC number is 2442345. The detailed crystallographic data and structure-refinement parameters are listed in Table 1.

2.3. Synthetic procedures

2.3.1. Syntheses of Sr-CuI-MOF. A mixture of 211.6 mg (1 mmol) of Sr(NO$_3$)$_2$, 100.0 mg (0.525 mmol) of CuI, 100.0 mg (0.598 mmol) of 3,5-pyridinedicarboxylic acid, 5.0 mL of *N,N*-dimethylformamide (DMF), 1.0 mL of acetonitrile (CH$_3$CN), and 1.0 mL of ethanol was sealed in a 8-mL glass vessel, which was heated at 100 °C for 2 days, and then cooled to room temperature. Yellow rod-shaped crystals were selected by hand, washed with absolute ethanol, and then dried in the air (90.23 mg, 20.4% yield based on HINA). Anal. calc: C, 30.18%; H, 2.97%; N, 7.65%. Found: C, 29.92%; H, 3.04%; N, 7.48%.

2.4. Density functional theory (DFT) calculations

Theoretical calculations of Sr-CuI-MOF were performed using the Vienna *Ab initio* Simulation Package (VASP) software based on DFT. The computational content included the density of states (DOS). For the electron–electron exchange–correlation process, the calculations employed the generalized gradient approximation (GGA) with the Perdew–Burke–Ernzerhof (PBE) exchange–correlation functional. To ensure sufficient accuracy, a plane-wave cutoff energy of 520 eV was selected. The convergence criterion for the self-consistent field (SCF) calculation was set to 1×10^{-5} eV, and the residual force criterion was set to 0.02 eV Å^{-1}. The theoretical calculation results were processed using the VASPKIT and visualization for electronic and structural analysis (VESTA) software.

2.5. Measurement of FL sensing

The as-made crystalline samples of Sr-CuI-MOF were manually ground to obtain fine powders. Then, 5 mg of powdered samples were dispersed in 2 mL of solvents, followed by ultrasonication for several minutes to obtain a stable emulsion. Then, the FL emulsion was stored at room temperature for 24 h to allow for

Table 1 Crystal data and structure refinement for Sr-CuI-MOF

Empirical formula	C$_{23}$H$_{27}$N$_5$O$_{11}$Sr$_2$CuI
Formula weight	915.17
Temperature/K	298(2)
Wavelength/Å	1.54178
Crystal system	Triclinic
Space group	$P\bar{1}$
a/Å	10.4830(1)
b/Å	12.6283(1)
c/Å	12.8952(1)
α/°	92.534(1)
β/°	105.099(1)
γ/°	103.871(1)
Volume/Å^3	1589.71(3)
Z	2
ρ_{calc} g cm^{-3}	1.912
Absorption coefficient/mm^{-1}	13.268
$F(000)$	892.0
Crystal size/mm^3	0.15 × 0.15 × 0.05
Reflections collected/unique	20 778/6584 [R_{int} = 0.0406]
Data/restraints/parameters	6584/400/463
Goodness-of-fit on F^2	1.062
Final R indexes [$I \geq 2\sigma\,(I)$]	$R_1{}^a$ = 0.0332, w$R_2{}^b$ = 0.0911
Final R indexes [all data]	$R_1{}^a$ = 0.0343, w$R_2{}^b$ = 0.0921

^{a} $R_1 = \sum ||F_o| - |F_c||/\sum |F_o|$. ^{b} w$R_2 = [\sum \mathrm{w}(F_o{}^2 - F_c{}^2)^2/\sum \mathrm{w}(F_o{}^2)^2]^{1/2}$.

22264 | *J. Mater. Chem. C*, 2025, **13**, 22263–22270

This journal is © The Royal Society of Chemistry 2025

adequate solvent exchange, after which it was transferred into a quartz cell of 1-cm width for FL measurement. For all measurements, the dispersed emulsions of Sr-CuI-MOF were excited at 420 nm while the corresponding emission wavelengths were monitored from 450 nm to 850 nm.

3. Results and discussion

3.1. Description of crystal structure

SCXRD analyses revealed that Sr-CuI-MOF crystallized in the triclinic system with space group $P\bar{1}$ (Table 1). Its asymmetric unit contained half a formula unit. That is, two crystallographically independent Sr atoms, one Cu atom, one I atom, two pdc^{2-} ligands, and three coordinated DMF molecules (Fig. S1). As illustrated in Fig. 1a, the Sr(1) center adopted an eight-coordinated geometry, bound by six deprotonated carboxylate oxygen atoms from four pdc^{2-} ligands and two oxygen atoms from two DMF molecules. By contrast, Sr(2) coordinated with seven carboxylate oxygen atoms from five pdc^{2-} ligands and one DMF molecule. All Sr–O bond lengths fell within the range 2.48–2.81 Å (Table S1), which are consistent with that of previous Sr-based MOFs.[26–28] The deprotonated pdc^{2-} ligands exhibited two distinct bridging modes (Fig. S2): the L1 ligand connected two Sr(1) and two Sr(2) atoms in a μ_4-η_2:η_2:η_1:η_1 coordination pattern, while L2 bridged two Sr(1) and three Sr(2) atoms via a μ_5-η_3:η_2:η_2:η_1 mode. This multidirectional coordination drove the formation of dinuclear $\{Sr_2(COO)_7(DMF)_3\}$ through sharing carboxylate groups between adjacent Sr^{2+} (Fig. 1a), which served as the secondary building unit (SBU) of the structure. The dinuclear SBUs were interconnected by μ_3-O(3) atoms to form a tetra-nuclear cluster and further bridged by μ_2-O(2) atoms, generating

a one-dimensional (1d) sr–o chain structure as a tertiary Building Unit (TBU) (Fig. 1b and c). CuI motifs within the framework of Sr-CuI-MOF featured a $[Cu_2I_2]$ cluster structure, and each Cu(I) coordinated to two pyridyl nitrogen atoms from two pdc^{2-} ligands, forming tetradentate-connected $[Cu_2I_2(pdc)_4]^{8-}$ functional units (Fig. 1d). Then, $[Cu_2I_2(pdc)_4]^{8-}$ units bridged the 1D Sr–O chains to form a 3D framework (Fig. 1e and f). Sr-CuI-MOF contained 1D channels along the a axis, occupied by terminally coordinated DMF molecules (Fig. 1e).

The phase purity of the as-made compound was confirmed by comparing the experimental PXRD with the simulated pattern generated from single-crystal diffraction data (Fig. S3 and S4). Sr-CuI-MOF appeared as yellow block-shaped crystals with an absorption edge at ~ 2.77 eV (Fig. S5). Thermogravimetric-differential thermogravimetric (TG-DTG) analyses revealed that it exhibited three distinct weight-loss peaks. The first peak near 60 °C was likely due to the volatilization of surface-adsorbed solvent molecules. Subsequent peaks at 280 °C and 330 °C corresponded to the dissociation of coordinated DMF molecules and structural collapse due to thermal decomposition of the organic ligands, respectively (Fig. S6a).

EDS-mapping confirmed the presence and homogeneous distribution of the primary constituent elements (Cu, I, Sr) within the Sr-CuI-MOF (Fig. S7 and S8). These findings were in agreement with the XPS data, which detected characteristic orbital signals corresponding to Sr 3d, Cu 2p, and I 3d, respectively. Notably, the binding energy analyses of the Cu 2p orbital revealed a 1^+ oxidation state for Cu^+, with no observable satellite peaks attributable to Cu^{2+} (Fig. S9). This result aligned with the structural data derived from SCXRD and elemental analyses, further corroborating the accuracy of the elemental composition and chemical valence states for Sr-CuI-MOF.
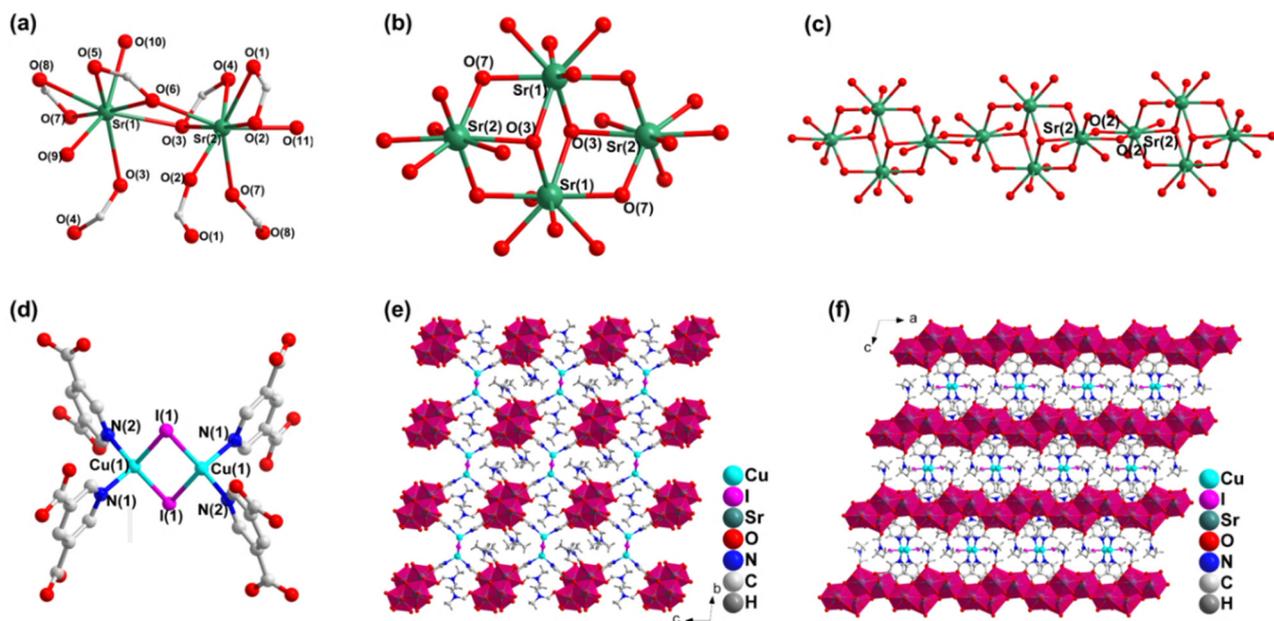

Fig. 1 Crystal structure of Sr-CuI-MOF. (a)–(c) Coordination environment for Sr^{2+}. (d) $[Cu_2I_2(pdc)_4]^{8-}$ building unit. (e) and (f) 3D framework of Sr-CuI-MOF viewed along the a and b axes directions, respectively.

This journal is © The Royal Society of Chemistry 2025

J. Mater. Chem. C, 2025, **13**, 22263–22270 | **22265**

3.2. Luminescence properties

At room temperature, Sr-CuI-MOF exhibited yellow–green fluorescence with a quantum yield of 11.88%. Under UV excitation at 420 nm, Sr-CuI-MOF reached a maximum emission peak at 545 nm (Fig. 2a and Fig. S10 and S11). Its fluorescence could be attributed to excitation at the center of the Cu_2I_2 clusters, which resulted from the charge transfer from ligand-to-metal and halide-to-metal. This behaviour is comparable to that observed in other previous copper–iodine based hybrid materials.[29–31] Variable-temperature fluorescence spectroscopy showed that Sr-CuI-MOF exhibited bright yellow–green fluorescence at 77 K, and its fluorescence intensity slowly diminished as the temperature gradually increased to 298 K (Fig. 2c). Fluorescence lifetime measurements indicated that, at 77 K, its fluorescence lifetime was 9.97 μs, nearly three-times that measured at 298 K (Fig. 2d). This occurrence aligns with other $Cu_xI_y(L)_z$ hybrids exhibiting thermally activated delayed fluorescence (TADF),[32–35] which can be explained by the decrease in thermally induced nonradiative decay. DFT calculations showed that the fluorescence of Sr-CuI-MOF was induced by the energy interactions between the inorganic $\{Cu_2I_2\}$ module and pdc^{2-} ligand. The calculated DOS of Sr-CuI-MOF included inorganic atomic states from the CuI component, specifically the Cu 3d atomic orbitals and I 5p atomic orbitals. This indicated that the emission resulted primarily from the energy transfer between the $\{Cu_2I_2\}$ module and pdc^{2-} ligand, acting as the main fluorescence center for Sr-CuI-MOF (Fig. 2e and f).

3.3. FL sensing

The as-prepared crystals of Sr-CuI-MOF were ground into a powder and dispersed in alcohol congeners and other commonly laboratory-used organic solvents to evaluate the FL-sensing capacity of Sr-CuI-MOF. As seen in Fig. 3a, Sr-CuI-MOF demonstrated a strong selective FL sensing to methanol, showing a noticeable transition in fluorescence colour from yellowish–green to orange (Fig. 3b). The emission colours of Sr-CuI-MOF dispersed in these solvents fell within the visible region, making it easy to visually identify selective FL sensing for methanol (Fig. 3c). Previously, FL sensing has relied regularly on the single-signal change in fluorescence intensity, such as quenching or enhancement. However, FL materials produce significant signal fluctuations if the concentration of the analytes exceeds acceptable limits. Fluorescence materials can exhibit considerable signal variations, resulting in misclassification.[21,36] Additionally, external factors impact fluorescence intensity, affecting the accuracy of the sensing array. Different from the previous reports, Sr-CuI-MOF showed a unique FL-quenching response to methanol with a visually discernible emission redshift, accompanied by a noticeable shift in emission towards longer wavelengths. This phenomenon makes it a suitable FL-sensing material for differentiating methanol from ethanol. By dispersing Sr-CuI-MOF in 2 mL of a mixture of methanol and ethanol over 24 h with different volume ratios (Fig. S12), linear changes in fluorescence intensity and shifts in emission wavelength in relation to the concentration of methanol were observed (Fig. 4b and c). As seen in Fig. 4a, the fluorescence intensity increased progressively with an increase in the volume ratio of methanol, while the maximum emission peak shifted to longer wavelengths. Comprehensive analyses revealed a strong linear correlation between the change in its emission wavelength and the percentage of the fluorescence intensity quenched with the relative ratio of methanol, and the correlation coefficient (R^2)
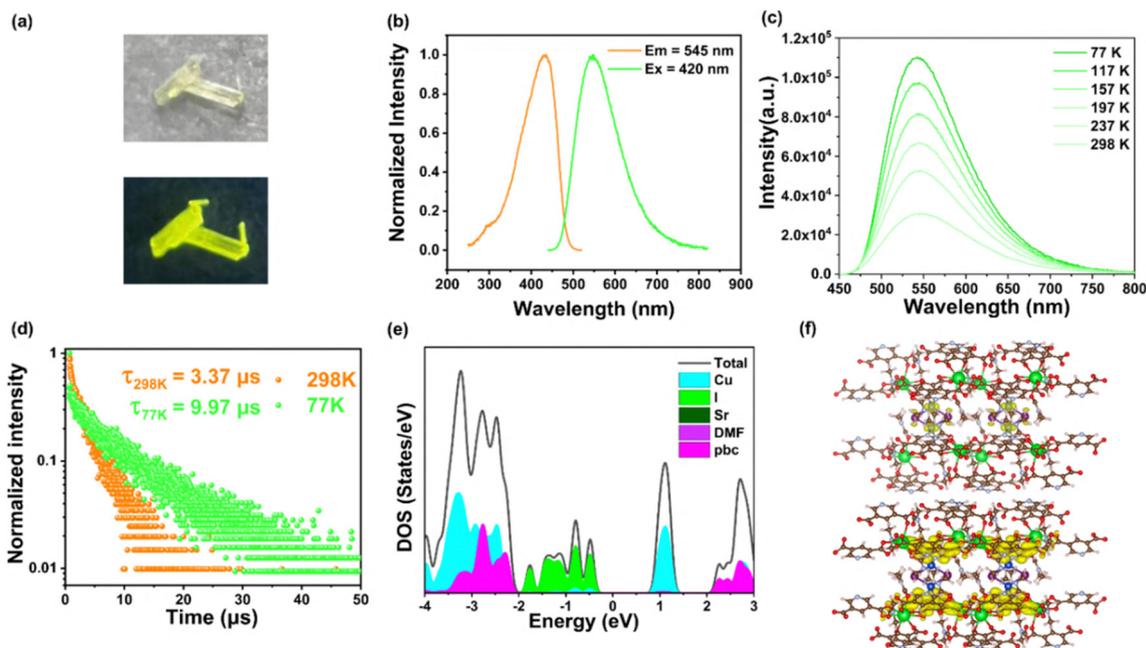

Fig. 2 (a) Photographs of crystals of Sr-CuI-MOF under daylight and 365-nm UV light at room temperature. (b) Excitation and emission spectra for as-made Sr-CuI-MOF. (c) Temperature-dependent fluorescence spectra for as-made Sr-CuI-MOF under 420-nm excitation. (d) Time-resolved fluorescence decay curves of Sr-CuI-MOF under 420-nm excitation at 77 K and 298 K (τ = lifetime). (e) Density of states plots of as-made Sr-CuI-MOF. (f) Plots of the valence band (VB; top) and conduction band (CB; bottom) for Sr-CuI-MOF.
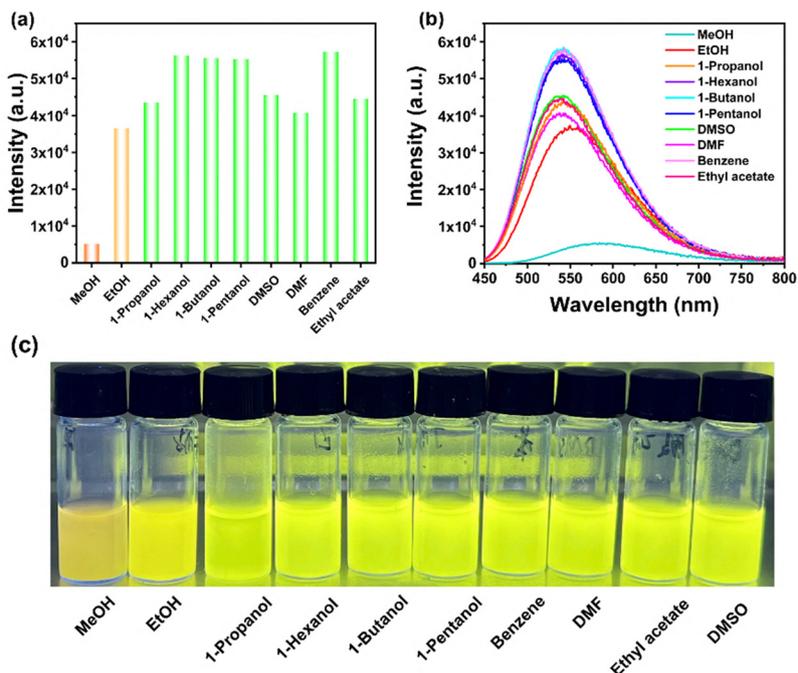
Fig. 3 (a) and (b) Fluorescence intensity and fluorescence spectra of Sr-CuI-MOF dispersed in methanol/ethanol mixed solutions with varied volume ratios. (c) Photographs of Sr-CuI-MOF dispersed in different VOCs under UV light.
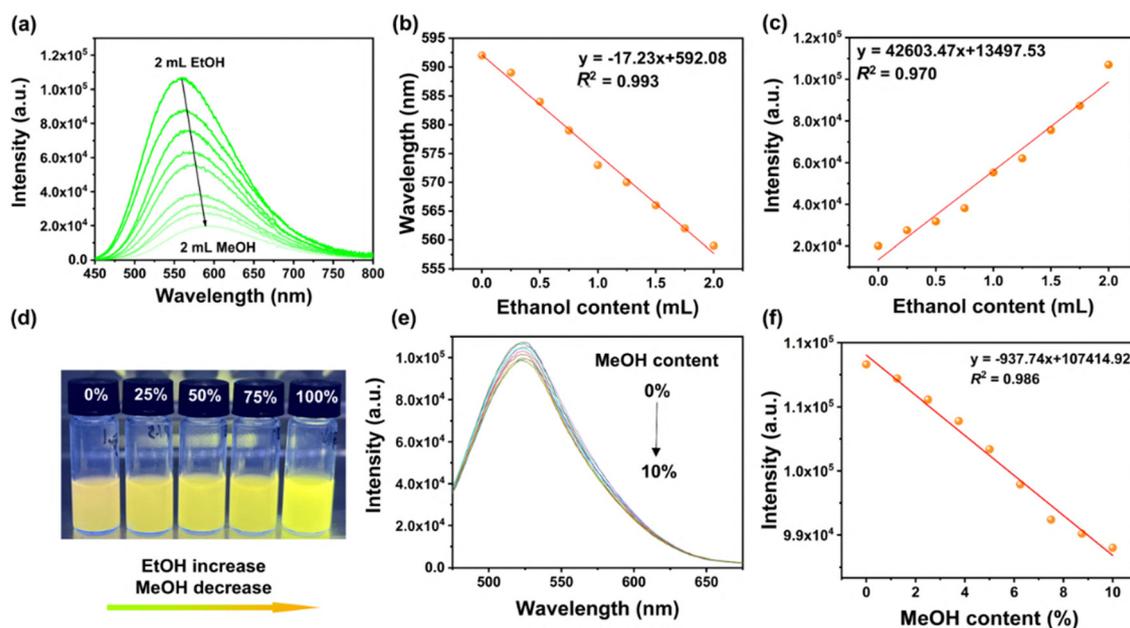

Fig. 4 (a) Fluorescence spectra of Sr-CuI-MOF dispersed in methanol and ethanol mixtures with different volume ratios. (b) Linear calibration curve between ethanol content and emission wavelength. (c) Linear calibration curve between ethanol content and fluorescence intensity. (d) Fluorescence photographs under 365-nm UV irradiation. (e) Fluorescence spectra of Sr-CuI-MOF dispersed in methanol and ethanol mixtures with methanol volume fractions ranging from 0% to 10%. (f) Linear correlation between ethanol content and fluorescence intensity.

reached 0.993 and 0.970, respectively (Fig. 4b and c). Consequently, its FL emulsion exhibited a distinct color shift from yellow to green under UV irradiation, making it easily noticeable to the naked eye (Fig. 4d). This dual-signal response enhanced the accuracy of the FL-sensing assay, and provided the detection system with remarkable selectivity, along with a clear visual representation (Fig. S13). Additionally, Sr-CuI-MOF could be used to accurately distinguish between methanol and ethanol mixtures at very low concentrations ($<10\%$ vol%) with a high R^2 of 0.986 by monitoring fluorescence changes (Fig. 4e and f). The FL-sensing performance of Sr-CuI-MOF was assessed for the detection of methanol in counterfeit wines (simulated by a mixture

This journal is © The Royal Society of Chemistry 2025

J. Mater. Chem. C, 2025, **13**, 22263–22270 | **22267**

of 85% ethanol and 15% water) as well as in contaminated ethanol fuel (represented by a mixture of 80% toluene and 20% ethanol). As illustrated in Fig. S14 and S15, this compound exhibited selective sensing capabilities to methanol, thereby confirming its specificity for methanol detection. This offers an effective and convenient method for assessing the quality of ethanol fuel and commercial wine.

Detecting volatile organic compounds (VOCs) through fluorescence in the gas phase often experiences low sensitivity because of the weak interactions (*e.g.*, hydrogen bonding, van der Waals forces) between the gaseous molecules and sensing materials. Notably, when as-made Sr-CuI-MOF was exposed to methanol and ethanol vapours, it exhibited a significant decrease in fluorescence (quenching efficiency: 95%) in response to methanol vapor, along with a 23-nm shift in emission from 545 nm to 568 nm (Fig. 5a and b). This significant redshift corresponds with its sensitivity trend in environments in which liquid detection occurs. In comparison, exposure to ethanol vapor resulted in only slight spectral changes (redshift <5 nm), which were not easily noticeable to the naked eye (Fig. 5c and d). However, the fluorescence switching between "on" and "off" states could be repeated for ≥5 cycles, with structural integrity preserved throughout repeat sensing experiments (Fig. S16). This result confirmed the reusability and repeatability of its sensing performances.

3.4. Mechanism of FL sensing

As illustrated in Fig. 6, the PXRD measurements of Sr-CuI-MOF confirmed that the FL sensing of methanol was not caused by structural collapse. The sensing performance of H_2pdc to

methanol was also conducted following the same method as that for Sr-CuI-MOF. As depicted in Fig. S17, the fluorescence intensity of H_2pdc remained almost unchanged whether treated with methanol or ethanol, demonstrating at the selective FL response of Sr-CuI-MOF to methanol did not originate from the organic ligand. LC–MS and elemental analyses were employed to understand the underlying mechanism. As shown in Fig. S18 and S19, LC–MS revealed distinctive DMF signals (positive ion mode, $m/z = 73.1 + 1 \,[M + H]^+$) to be present in the methanol-soaked solution of Sr-CuI-MOF. In contrast, DMF-related signals were not detected in the sample dispersed in *n*-butanol. This result indicated the DMF trapped in Sr-CuI-MOF could be exchanged by methanol, which could be released and analyzed by LC–MS. Moreover, elemental analyses indicated that Sr-CuI-MOF treated with post-*n*-butanol immersion retained nearly identical levels of carbon (C: 29.85%) and nitrogen (N: 6.99%) compared with that in the original sample (C: 29.92%; N: 7.48%). The Sr-CuI-MOF sample soaked in methanol showed a notable decrease in the amounts of carbon (21.47%) and nitrogen (4.14%), suggesting that the terminally coordinated DMF was replaced by methanol. The findings discussed above suggest that the FL quenching and redshift observed specifically in response to methanol may have been due to the partial dissociation of DMF molecules that were coordinated to Sr atoms in Sr-CuI-MOF, which are then replaced by methanol molecules (Fig. 6).[37–40] This dynamic replacement of guests changes the local electronic surroundings of $Cu_2I_2(pdc)_4$ luminescent centers which, in turn, affects their metal/halogen-to-ligand charge transfer emission characteristics, and leads to selective FL sensing.
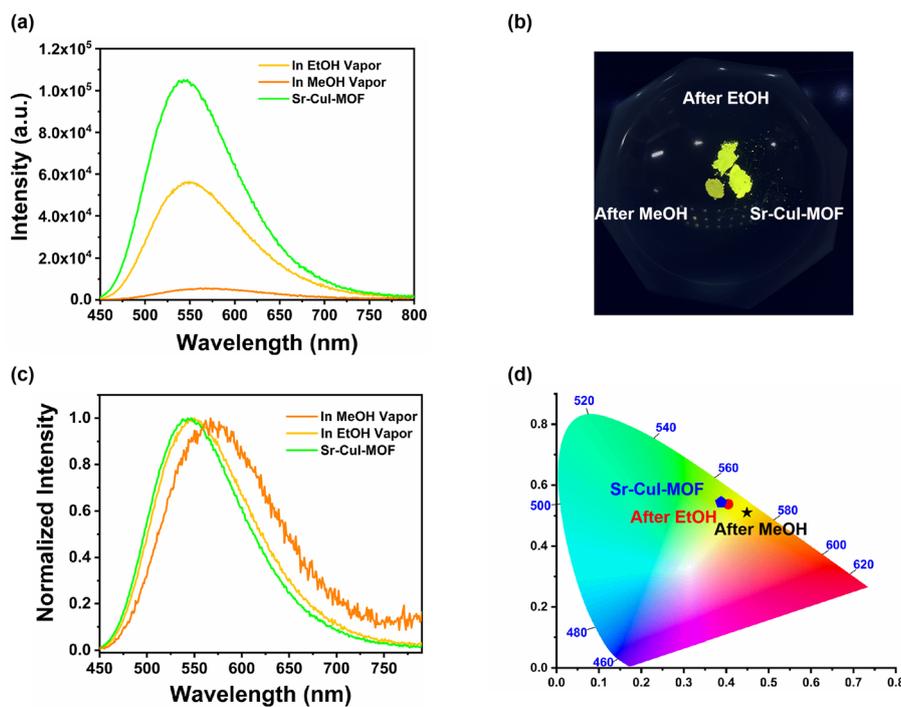

Fig. 5 (a) Fluorescence emission spectra of Sr-CuI-MOF before and after exposure to methanol and ethanol vapors. (b) Luminescence photographs for as-made Sr-CuI-MOF before and after exposure to methanol and ethanol vapors. (c) Normalized fluorescence emission spectra for as-made Sr-CuI-MOF before and after exposure to methanol and ethanol vapors. (d) CIE chromaticity of Sr-CuI-MOF under methanol and ethanol vapors.
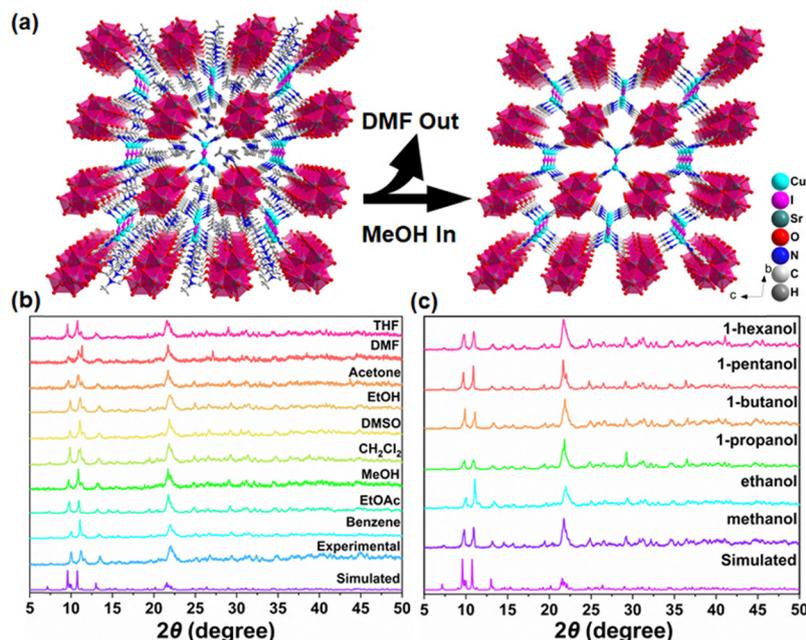
22268 | *J. Mater. Chem. C*, 2025, **13**, 22263–22270

This journal is © The Royal Society of Chemistry 2025

Fig. 6 (a) FL-sensing mechanism for Sr-CuI-MOF. (b) and (c) PXRD measurements for Sr-CuI-MOF immersed in different solvents and alcohols over 12 h.

4. Conclusions

A 3D Sr-CuI-MOF with $[Cu_2I_2(pdc)_4]^{8-}$ modules as building blocks and luminescent components is presented. It demonstrated a preference for FL sensing of methanol compared with other alcohols. As a responsive FL-sensing material, Sr-CuI-MOF could selectively and sensitively detect methanol in comparison with ethanol by reducing its fluorescence intensity and altering the emitted colours, allowing for easy identification of methanol over ethanol by the naked eye. The sensing mechanism was examined through various experimental characterizations. This work provides a valuable reference for the design of novel MOF-sensing materials utilizing $\{Cu_2I_2\}$-L modules as foundational elements and luminescent centers.

Conflicts of interest

There are no conflicts of interest to declare.

Data availability

The data supporting this article have been included as part of the supplementary information (SI). Supplementary information: PXRD patterns, more crystal structural details, PL spectra, TG curve. See DOI: **https://doi.org/10.1039/d5tc02781k**.

CCDC 2442345 contains the supplementary crystallographic data for this paper.[41]

Acknowledgements

References

1 J. P. Potier, *Rev. Med. Liege*, 1990, **45**, 331.
2 A. Jangjou, M. Moqadas, L. Mohsenian, H. Kamyab, S. Chelliapan, S. Alshehery, M. A. Ali, F. Dehbozorgi, K. K. Yadav, M. Khorami and N. Z. Jelyani, *Environ. Res.*, 2023, **228**, 115886.
3 K. Jahan, D. Mahmood and M. Fahim, *J. Pharm. BioAllied Sci.*, 2015, **7**, 60.
4 B. Inman, J. K. Maddry, P. C. Ng, A. Koyfman and B. T. Long, *Am. J. Emerg. Med.*, 2023, **67**, 29.
5 J. van den Broek, S. Abegg, S. E. Pratsinis and A. T. Güntner, *Nat. Commun.*, 2019, **10**, 4220.
6 S. Y. Jeong and J. Jang, *Chem. Eng. J.*, 2025, **507**, 160614.
7 F. V. C. Kock, T. C. Rocha, G. M. Araújo, F. R. Simões, L. A. Colnago and L. Barbosa, *Fuel*, 2019, **258**, 116158.
8 H. J. R. Caleja-Ballesteros and J. I. Ballesteros, *Food Addit. Contam.: Part A*, 2025, **42**, 159.
9 C. M. Gong, W. Huang, J. J. Liu, F. X. Wei, J. W. Yu, X. K. Si, F. H. Liu and Y. F. Li, *Fuel*, 2018, **221**, 188.
10 Y. M. Zhang, S. Yuan, G. Day, X. Wang, X. Y. Yang and H. C. Zhou, *Coord. Chem. Rev.*, 2018, **354**, 28.
11 Y. Y. Cai, T. Dong, Z. H. Bian, H. Liu, X. Liu and A. H. Liu, *Coord. Chem. Rev.*, 2025, **529**, 216470.
12 D. Wu, A. C. Sedgwick, T. Gunnlaugsson, E. U. Akkaya, J. Yoon and T. D. James, *Chem. Soc. Rev.*, 2017, **46**, 7105.
13 S. Y. Wu, H. Min, W. Shi and P. Cheng, *Adv. Mater.*, 2020, **32**, 1805871.
14 Y. Y. Cui, H. J. Lu, H. L. Hou, Y. Y. Bai, J. P. Yang, Y. R. Li, J. Qiu, S. O. Wang and J. Lin, *Angew. Chem., Int. Ed.*, 2024, **63**, e202410453.
15 F. F. Lang, L. L. Zhang, Y. Li, X. J. Xi, J. D. Pang, W. J. Zheng, H. C. Zhou and X. H. Bu, *Angew. Chem., Int. Ed.*, 2025, **64**, e202422517.

This journal is © The Royal Society of Chemistry 2025

J. Mater. Chem. C, 2025, **13**, 22263–22270 | **22269**

16 W. B. Li, Y. Wu, X. F. Zhong, X. H. Chen, G. Liang, J. W. Ye, Z. W. Mo and X. M. Chen, *Angew. Chem., Int. Ed.*, 2023, **62**, e202303500.

17 T. Y. Luo, P. Das, D. L. White, C. Liu, A. Star and N. L. Rosi, *J. Am. Chem. Soc.*, 2020, **142**, 2897.

18 D. M. Chen, C. X. Sun, Y. Peng, N. N. Zhang, H. H. Si, C. S. Liu and M. Du, *Actuator B: Chem.*, 2018, **265**, 104.

19 R. R. F. Fonseca, R. D. L. Gaspar, I. M. Raimundo and P. P. J. Lu, *Rare Earths*, 2019, **37**, 225.

20 M. Sangeetha, J. Pitchaimani and V. Madhu, *Anal. Methods*, 2025, **17**, 3856.

21 T. Wiwasuku, J. Othong, J. Boonmak, V. Ervithayasuporn and S. Youngme, *Dalton Trans.*, 2020, **49**, 10240.

22 H. M. Wang, H. P. Liu, T. S. Chu, Y. Y. Yang, Y. S. Hu, W. T. Liu and S. W. Ng, *RSC Adv.*, 2014, **4**, 14035.

23 J. Wang, M. Jiang, L. Yan, R. Peng, M. J. Huangfu, X. X. Guo, Y. Li and P. Y. Wu, *Inorg. Chem.*, 2016, **55**, 12660.

24 Z. Jin, H. M. He, H. Y. Zhao, T. Borjigin, F. X. Sun, D. M. Zhang and G. S. Zhu, *Dalton Trans.*, 2013, **42**, 13335.

25 G. M. Sheldrick, *Acta Crystallogr. Sect. C Struct. Chem.*, 2015, **71**, 3–8.

26 C. Wang, X. J. Zhang, L. N. Zhao, T. Zhang, F. Y. Bai, L. X. Sun and Y. H. Xing, *ACS Appl. Mater. Interfaces*, 2024, **16**, 45214.

27 M. Niemiec, J. J. Zakrzewski, M. Reczynski and S. Chorazy, *Adv. Opt. Mater.*, 2025, 2403564.

28 X. L. Guo, N. S. Zhu, S. P. Wang, G. H. Li, F. Q. Bai, Y. Li, Y. H. Han, B. Zou, X. B. Chen, Z. Shi and S. H. Feng, *Angew. Chem., Int. Ed.*, 2020, **59**, 19716.

29 Y. N. Zhao, Q. Yang, B. H. Yao, R. Y. Cao, H. Zhang, S. L. Wei, D. H. Wei, K. Li, Y. B. Si and S. Q. Zang, *Angew. Chem., Int. Ed.*, 2025, e202500481.

30 Q. C. Peng, R. Y. Cao, Q. Yang, Y. B. Si, J. W. Yuan, Y. Y. Lei, Z. Y. Wang, Q. Tang, K. Li and S. Q. Zang, *Adv. Mater.*, 2025, 2504425.

31 Y. J. Kong, Z. P. Yan, S. Li, H. F. Su, K. Li, Y. X. Zheng and S. Q. Zang, *Angew. Chem., Int. Ed.*, 2020, **59**, 5336.

32 Y. Z. Wang, T. H. Zhang, W. J. Zhao, W. D. Xu, Z. B. Wu, Y. D. Suh, Y. Z. Zhang, X. W. Liu and W. Huang, *Angew. Chem., Int. Ed.*, 2024, **64**, e202413672.

33 J. J. Wang, C. Chen, W. G. Chen, J.-S. Yao, J. N. Yang, K. H. Wang, Y. C. Yin, M. M. Yao, L. Z. Feng, C. Ma, F. J. Fan and H. B. Yao, *J. Am. Chem. Soc.*, 2020, **142**, 3686.

34 K. H. Song, M. Peng, J. J. Wang, L. Z. Feng, Y. C. Yin, Y. H. Song, X. C. Ru, Y. P. Xie, G. Z. Zhang, Z. T. Deng and H. B. Yao, *J. Am. Chem. Soc.*, 2024, **146**, 34199.

35 H. B. Li, J. Yang, Q. Q. Wang, H. Tong, J. L. Zhu, W. Liu and G. F. Ouyang, *Adv. Opt. Mater.*, 2024, **12**, 2400364.

36 M. E. Besheli, R. Rahimi, Y. D. Farahani and V. Safarifard, *Inorg. Chim. Acta*, 2019, **495**, 11895.

37 Y. W. Tang, A. Kourtellaris, A. J. Tasioloulos, S. J. Teat, D. Dubbeldam, G. Rothenberg and S. Tanase, *Inorg. Chem. Front.*, 2018, **5**, 541.

38 P. C. Guo, Z. Y. Chu, X. M. Ren, W. H. Ning and W. Q. Jin, *Dalton Trans.*, 2013, **42**, 6603.

39 J. Guo, X. M. Xue, H. B. Yu, Y. L. Duan, F. F. Li, Y. Lian, Y. Liu and M. T. Zhao, *J. Mater. Chem. A*, 2022, **10**, 19320.

40 D. Guo, C. M. Liang, K. Chiu and W. K. Wang, *Z. Anorg. Allg. Chem.*, 2021, **647**, 119.

41 CCDC 2442345: Experimental Crystal Structure Determination, 2025, DOI: **10.5517/ccdc.csd.cc2mzgbf**.

22270 | *J. Mater. Chem. C*, 2025, **13**, 22263–22270

This journal is © The Royal Society of Chemistry 2025